A&A 581, A99 (2015)
DOI: 10.1051/0004-6361/201526364

Astronomy & Astrophysics

Spectroscopic identification of 25 disk galaxy candidate gravitational lenses in the SDSS

P. Focardi and E. Rossetti

Dipartimento di Fisica e Astronomia, Universitá di Bologna, 40126 Bologna, Italy
e-mail: [paola.focardi;emanuel.rossetti]@unibo.it

Received 20 April 2015 / Accepted 16 July 2015

ABSTRACT

Context. Galaxy-scale gravitational lenses are powerful tools, which can be used to address major astrophysical questions that are still open. They can be identified either through imaging or through spectroscopy, which is less efficient than imaging but offers the major advantage of having both source and deflector red shift previously measured at discovery. Spectroscopic identification requires huge data sets of high spectral quality, such as the SDSS, and has so far focused on early-type galaxies, as the most massive galaxies are found among them.
Aims. We aimed to perform spectroscopic identification of disk galaxies acting as gravitational lenses.
Methods. We have selected about 300 000 galaxy spectra with $EW(\mathrm{H}_\alpha) \leq -10$ Å from the SDSS DR 8. On these spectra, we ran our original code RES, which is a fast, reliable tool able to provide a red-shift measure and to identify discordant red-shift systems if present. We have required RES to identify only systems based on a minimum number of four emission lines. We have inspected all the (54) SDSS images of the double z systems identified by RES and discarded systems for which z duplicity could be easily ascribed to the presence of two distinct objects. The remaining 25 systems, for which double z is very likely to be due to the gravitational lensing phenomenon, constitute our sample.
Results. For each gravitational lens candidate system, we provide SDSS identification and image emission lines detected by RES and activity classification, when derivable. The disky nature of our candidate lenses is confirmed by their images, stellar mass estimates, $g - r$ rest-frame colours and occurrence of star burst phenomena.

Key words. gravitational lensing: strong – techniques: spectroscopic

1. Introduction

Galaxy-scale gravitational lenses are powerful tools that can be used to address major astrophysical open questions, such as the mass spatial distribution within galaxies (Kochanek et al. 1991; Rusin & Kochanek 2005; Koopmans et al. 2006; Jiang & Kochanek 2007), the geometry, content, and kinematics of the Universe (Refsdal 1964; Oguri 2007), and the nature of objects that are too far away to be observed directly (see e.g. Marshall et al. 2007; Bunker et al. 2000; Smail et al. 2007; Allam et al. 2007; Poindexter et al. 2008). If the lensed object is a galaxy too, then more constraints on the lens mass distribution can be obtained (Kochanek et al. 2001; Koopmans 2005).

Identification of galaxy-scale gravitational lenses may be done either through imaging, looking for distorted, amplified, and multiplied images of the lensed object in the close neighbourhood of massive galaxies, or through spectroscopy, looking for higher red-shift emission lines in the spectrum of the candidate lensing galaxy. The imaging approach is more efficient than the spectrosopy approach, which however offers a major advantage: source and deflector red shift (and thus the basic lensing geometry) are already determined upon discovery. Not only that, spectroscopically detected candidates may turn out to be undetectable through broadband imaging because of both the faintness and closeness of the source relative to the lens. In this respect, a search for discrepant emission features in galaxy spectra can potentially lead to a sample of gravitational lens systems that would not be discovered in broadband imaging searches because of the faintness of the source relative to the lens.

Availability of large sets of high quality data, such as the Two-degree-Field Galaxy Redshift Survey (2dFGRS, Colless et al. 2001), and the Sloan Digital Sky Survey (SDSS, York et al. 2000), made a number of studies devoted to spectroscopic identification of galaxy-scale gravitational lensing phenomenon feasible (Hewett et al. 2000; Bolton et al. 2004, 2006, 2008; Treu et al. 2006; Koopmans et al. 2006; Gavazzi et al. 2007, 2008; Willis et al. 2005, 2006; Brownstein et al. 2012). All of these studies, however, concentrated on large, massive early-type galaxies as they have the largest probability of acting as gravitational lenses on background sources, having the right combination of distance and impact parameter. Because of their smaller masses, spiral galaxies are expected to account for only 10% to 20% of gravitational lenses (Turner et al. 1984; Fukugita & Turner 1991; Kochanek 1993, 1996; Maoz & Rix 1993; Keeton & Kochanek 1998) and actually so far, only a few disk galaxy lenses are known (Bolton et al. 2008; Feron et al. 2009).

Lensing geometry in disk galaxies is due to the combined contribution of bulge, disk, and DM halo within the Einstein radius and can be used to obtain an independent estimate of the M/L ratio, breaking the so-called disk halo degeneracy (Maller et al. 2000; Dutton et al. 2011). With the aim to detect disk galaxy gravitational lenses, we selected from the SDSS-III data release 8 (Aihara et al. 2011) 335 681 galaxy spectra that have

H_α Equivalent Width (EW) less than or equal to −10 Å. This constraint ensured the sample would be mostly populated by disk galaxies later than Sb (Kennicutt 1998).

On this sample we run our original code Redshift for Emission line Spectra (RES), which is a fast reliable tool, able to provide a red shift based on the identification of emission lines. It is thus straightforward for RES to identify discordant z systems in the same spectrum, when present. To avoid contamination by fake z systems, which might arise from spurious features lying by chance in the right z place, we asked RES to identify only z systems with at least four emission lines. From the 54 spectra identified by RES with a double z component, we discarded the 29 for which z duplicity could be unambiguously attributed to the combined contribution of different objects laying within the 3″ diameter of the fiber feeding the SDSS spectrograph. We were thus left with 25 previously unknown gravitational lens candidate systems (GLCSs), which are the object of this paper. The paper is structured as follows: in Sect. 2 the code RES is briefly described, in Sect. 3 the GLCS sample is presented, in Sect. 4 the activity type is derived for a large fraction of the sample and the conclusions are drawn in Sect. 5.

2. The code

We developed RES with the aim of building a reliable tool able to deal automatically with large amount of spectral data and to provide the red-shift measure simply on the basis of the detected (and identified) emission lines. The first version of RES dates back to 2011 and was quite soon branched into Redshift Estimate for Slitless Spectra (RESS) because of the need to assess the expected performances of NISP instrument of Euclid ESA Mission (Majerotto et al. 2012; Roche et al. 2012). In the meantime, we continued working on original RES, optimizing its performances and translating it from the original Tcl/Tk scripting environment into Python programming language.

The RES philosophy is simple: the code detects emission lines (above a given threshold) and then looks for the z value for which the detected lines matches the z shifted position of a list of rest-frame emission lines, which must be given in input. The input list is supposed to contain a reasonable number of features, which must however accord with the spectral wavelength range and quality of data. Because of the good quality of SDSS spectra and also taking the constraint that we have imposed on H_α EW into account, we have inserted in the input list the ten most frequently detected emission lines in galaxy spectra, namely [O II]$_{3727}$, H_β, [O III]$_{4959}$, [O III]$_{5007}$, [O I]$_{6300}$, [N II]$_{6549}$, H_α, [N II]$_{6584}$, [S II]$_{6717}$, [S II]$_{6731}$.

The frequency of the above mentioned emission lines, however, does not imply that they will always be present or always be the strongest features in each spectrum, as there might be spectra showing strong emission lines that are not included in the list and spectra of low S/N in which spurious features deriving, for example, from badly subtracted sky lines, may be stronger than the real emission features. Thus, to ensure no loss of valuable information, it is advisable to make RES detect a number of candidate emission lines which is between two and three times the size of the input list. (This number must be provided by the user and we have set it equal to 30.)

The emission line detection algorithm of RES starts looking for peaks above a threshold that has a starting value of 5σ above the spectrum continuum, and then proceeds modifying the threshold and repeating the detection until it finds a number of emission lines that best approximates the number desired by the user.

Table 1. RES reliability as a function of identified emission lines.

n_L	N	N ($\lvert\Delta z\rvert \le 0.001$)	$\langle\Delta z\rangle$	$\sigma_{\langle\Delta z\rangle}$
2	14 418	7 168	4.5×10^{-5}	1.9×10^{-4}
3	17 242	16 587	2.6×10^{-5}	1.5×10^{-4}
4	23 223	23 206	1.9×10^{-5}	1.2×10^{-4}

After detection of the candidate emission lines, RES cross checks their position with the z shifted position of the input rest-frame list looking for possible z matches, which must occur (within a user required tolerance δz) for a minimum number of two emission lines. A z coincidence of only two lines, however, may arise from spurious features (spectral artifacts, badly subtracted sky lines, etc.) or from a real line with a spurious feature lying by chance in the right z place, an effect which is expected to increase with decreasing spectral S/N. Thus, whenever RES finds different values for z for the same spectrum, it sorts them as a function of decreasing number of identified emission lines, keeping as good only the first z of the list (as it is the one with highest probability of being the true red shift value).

The code RES may also be asked to identify further emission lines that are not included in the input list. This option, which can be activated by the user when starting the program, has been thought for spectra with a lot of emission lines. A second list of rest-frame emission lines can be provided by the user (containing for example further lines of the Balmer series, [Ne III]$_{3868}$, He I$_{4471}$, He I$_{5875}$, [O I]$_{6363}$, etc.), together with a number indicating the score (in terms of identified emission lines) needed by each spectrum to have this second identification run. It is only advisable to make RES look for further lines when the majority of lines have been identified in the first identification run.

At the end of the run, RES provides in output, for each spectrum, the value for z obtained averaging all z of identified emission lines (which are provided as well). It is quite easy and feasible to make the code provide possible discrepant z values as well; these are likely to be real because of the combined contribution (in the same spectrum) of different objects. That is what we did, asking RES to provide only discrepant z, based on a minimum number of four emission lines, a choice that resulted in a contamination by fake z systems equal to zero.

Contamination by fake z systems may approach 50% when z_{RES} is only based on two lines, as illustrated in Table 1, which shows the result of our running RES on the 335 681 galaxy spectra, which constitute our starting sample. Column 1 lists the number of emission lines identified by RES; Col. 2 lists the corresponding total number of spectra; Col. 3 lists the number of spectra for which z_{RES} and z_{SDSS} are in very good agreement (i.e. $|\Delta z| = |z_{RES} - z_{SDSS}| \le 0.001$); Cols. 4 and 5 show the average value of Δz (computed on the sample of data in Col. 3) and its RMS ($\sigma_{\langle\Delta z\rangle}$), respectively.

Comparing Cols. 3 and 2, we see that the z agreement between z_{RES} and z_{SDSS} is already very good (96%) when RES manages to identify three emission lines and reaches 99.9% when z_{RES} relies on four emission lines. The 17 spectra failing the criterion of Col. 3 are characterized (as expected) by a very low S/N.

3. Gravitational lens candidate systems

As a result of its run on the original sample (335 681 SDSS galaxy spectra having a H_α $EW \le -10$ Å) RES returned 54 spectra showing a double z component (each characterized by a minimum number of four identified emission lines.

Table 2. Gravitational lens candidates systems.

GLCS	Identifier	z_L	z_S	z_{SDSS}	z_{NED}	$\Delta\theta$
1	SDSS J014659.99+135213.8	0.0644	0.1971	0.1974	0.1972[a]	0.4
2	SDSS J024933.37-080549.4	0.0298	0.2695	0.2695	0.2696[b]	0.5
3	SDSS J085107.30+150343.4	0.0699	0.2061	0.0699	0.0698[c]	0.4
4	SDSS J085620.98+650324.0	0.0675	0.3389	0.0675	0.0675	0.5
5	SDSS J100143.50+133212.4	0.0337	0.0846	0.0845	0.0846	0.3
6	SDSS J102403.67+245139.3	0.1062	0.1961	0.1062	0.1960[d]	0.3
7	SDSS J104356.09+044443.4	0.1511	0.3323	0.1510	0.3323	0.3
8	SDSS J110840.85+190836.4	0.0677	0.1027	0.1028	0.1030	0.2
9	SDSS J112202.44+162917.0	0.1062	0.1576	0.1062	0.1062	0.2
10	SDSS J114553.15+410049.7	0.0330	0.1641	0.0329	0.1641[e]	0.5
11	SDSS J115537.16+631101.6	0.1219	0.1485	0.1485	0.1485[f]	0.1
12	SDSS J121925.33+273255.0	0.0801	0.1047	0.0800	0.0802	0.1
13	SDSS J131105.31+022528.3	0.0674	0.1186	0.0675	0.0674	0.2
14	SDSS J141546.21-011112.5	0.0499	0.1493	0.0499	0.0499	0.4
15	SDSS J145237.94+091835.4	0.0547	0.1627	0.0547	0.0546[g]	0.4
16	SDSS J150032.76+262539.7	0.0632	0.0842	0.0842	0.0842	0.1
17	SDSS J161037.33+000832.7	0.0627	0.1074	0.1074	0.1075[h]	0.2
18	SDSS J161527.44+270706.1	0.0455	0.0964	0.0964	0.1129	0.3
19	SDSS J165958.80+355609.4	0.0827	0.2940	0.2940	0.2939	0.4
20	SDSS J210607.89-004756.6	0.0348	0.1146	0.0348	0.0347	0.4
21	SDSS J214425.43+114423.0	0.0259	0.2184	0.0259	0.0259[i]	0.5
22	SDSS J215813.68+003228.7	0.0557	0.1326	0.0557	0.1976	0.3
23	SDSS J232943.08+152219.9	0.0463	0.1029	0.1028	0.1028	0.3
24	SDSS 233129.22+005217.1	0.1393	0.3158	0.3157	0.3158	0.3
25	SDSS J233505.83-101625.2	0.0596	0.2105	0.0595	0.0595	0.4

Notes. The letter next to z_{NED} value indicates presence (in NED) of a discrepant value for z. All these cases are extensively illustrated below. [(a)] The value indicated by NED refers to SDSS DR 2 and is derived from absorption lines. The discrepant value ($z = 0.0644$) refers to the same DR and is derived from emission lines. [(b)] The value indicated by NED refers to SDSS DR 2 and is derived from absorption lines. The discrepant value ($z = 0.0298$) refers to the same DR and is derived from emission lines. [(c)] The value indicated by NED refers to SDSS DR 6 and is derived from absorption lines. The discrepant value ($z = 0.4444$), which is mistake, refers to the same DR and is derived from emission lines. [(d)] The value indicated by NED refers to SDSS DR 6 and is derived from absorption and emission lines. The discrepant value ($z = 0.1062$) refers to the same DR and is derived from absorption lines. [(e)] The value indicated by NED refers to SDSS DR 4 and is derived from emission lines. The discrepant value ($z = 0.0331$) refers both to the same DR and to DR 5. In the former case, it is derived from absorption lines, in the latter case it is derived from both absorption and emission lines. [(f)] The value indicated by NED refers to SDSS DR 2 and is derived from absorption and emission lines. The discrepant value ($z = 0.1221$) refers to the same DR and is derived from emission lines. [(g)] The value indicated by NED refers to SDSS DR 6 and is derived from absorption lines. The discrepant value ($z = 0.1623$) refers to the same DR and is derived from emission lines. [(h)] The value indicated by NED refers to SDSS DR 2 and is derived from absorption lines. The discrepant value ($z = 0.0628$) refers to the same DR and is derived from emission lines. [(i)] The value indicated by NED refers to SDSS DR 2 and is derived from absorption lines. The discrepant value ($z = 0.2183$) refers to the same DR and is derived from emission lines.

Visual inspection of all 54 SDSS spectra allowed us to confirm the reality of all identified features and as a consequence z duplicity in each spectrum.

The presence of a discordant z system, however, is not always a signature of the gravitational lensing phenomenon. We thus checked all SDSS images and discarded 29 systems for which double z component could be unambiguously attributed either to physically related (interacting) galaxies or to galaxies that only appear close in projection. For the remaining 25 systems, which constitute our sample, z duplicity is very likely to arise from the gravitational lensing phenomenon.

For each of these GLCSs, Table 2 reports a sequential number increasing with RA (Col. 1), the SDSS identifier (Col. 2), RES z measure of the lensing (z_L) and lensed (z_S) galaxy (Cols. 3 and 4), z value provided by the SDSS (Col. 5), z value provided by NED (Col. 6), and a very rough estimate of the expected angular scale ($\Delta\theta$) for any lensing in each system (Col. 7). The value in Col. 7 is actually the Einstein radius derived under the assumption of a Singular Isothermal Ellipsoid (SIE) lens model (Kormann et al. 1994; Kassiola & Kovner 1993), which we computed as $\Delta\theta = 4\,\pi\,(\sigma_v^2/c^2)\,(D_{LS}\,/D_S)$, with D_{LS} and D_S being the angular-diameter distances from lens to source and from observer to source (which we derived assuming $\Omega_M = 0.3$, $\Omega_\Lambda = 0.7$ and $H_0 = 70\,\mathrm{km\,s^{-1}\,Mpc^{-1}}$) and σ_v is the galaxy velocity dispersion ($\sigma_v = v_c/\sqrt{2}$), which we derived assuming a value of 200 km s^{-1} for the rotation velocity v_c.

From Table 2, we see that z_{SDSS} either matches z_L (11 cases) or with z_S (14 cases) and that z_{NED} matches z_{SDSS} in all but five cases (GLCS 6, 7, 10, 18, 22). For the first three objects, z_{NED} is in good agreement with z_S, while for GLCS 18 and 22 z value reported by NED is clearly a mistake.

We see also that in nine cases (including the previously mentioned GLCS 6 and 10) z_{NED} is accompanied by a letter, indicating that discrepant z values for those objects can be found by careful check of all z values available in NED. These discrepant z values and details concerning how they have been derived are given in the footnotes of Table 2, revealing that in most (8/9) cases the SDSS z measure algorithm had managed to detect the

Table 3. Emission lines in GLC components.

GLC	n_{EL}	Emission lines
1L	9	[O II]$_{3727}$, H$_\beta$, [O III]$_{4959}$, [O III]$_{5007}$, [N II]$_{6549}$, H$_\alpha$, [N II]$_{6584}$, [S II]$_{6717}$, [S II]$_{6731}$
1S	10	[O II]$_{3727}$, [Ne III]$_{3868}$, H$_\beta$, [O III]$_{4959}$, [O III]$_{5007}$, [N II]$_{6549}$, H$_\alpha$, [N II]$_{6584}$, [S II]$_{6717}$, [S II]$_{6731}$
2L	7	[O II]$_{3727}$, H$_\beta$, [O III]$_{5007}$, H$_\alpha$, [N II]$_{6584}$, [S II]$_{6717}$, [S II]$_{6731}$
2S	8	[O II]$_{3727}$, H$_\beta$, [O III]$_{4959}$, [O III]$_{5007}$, H$_\alpha$, [N II]$_{6584}$, [S II]$_{6717}$, [S II]$_{6731}$
3L	6	[O II]$_{3727}$, H$_\beta$, H$_\alpha$, [N II]$_{6584}$, [S II]$_{6717}$, [S II]$_{6731}$
3S	6	H$_\beta$, [O III]$_{5007}$, [N II]$_{6549}$, H$_\alpha$, [N II]$_{6584}$, [S II]$_{6717}$
4L	8	[O II]$_{3727}$, H$_\beta$, [O III]$_{5007}$, [N II]$_{6549}$, H$_\alpha$, [N II]$_{6584}$, [S II]$_{6717}$, [S II]$_{6731}$
4S	5	[O II]$_{3727}$, H$_\beta$, [O III]$_{4959}$, [O III]$_{5007}$, H$_\alpha$
5L	7	[O II]$_{3727}$, H$_\beta$, [O III]$_{4959}$, [O III]$_{5007}$, H$_\alpha$, [S II]$_{6717}$, [S II]$_{6731}$
5S	10	[O II]$_{3727}$, H$_\beta$, [O III]$_{4959}$, [O III]$_{5007}$, [O I]$_{6300}$ [N II]$_{6549}$, H$_\alpha$, [N II]$_{6584}$, [S II]$_{6717}$, [S II]$_{6731}$
6L	8	[O II]$_{3727}$, H$_\beta$, [O III]$_{5007}$, [N II]$_{6549}$, H$_\alpha$, [N II]$_{6584}$, [S II]$_{6717}$, [S II]$_{6731}$
6S	7	[O II]$_{3727}$, [O III]$_{5007}$, [N II]$_{6549}$, H$_\alpha$, [N II]$_{6584}$, [S II]$_{6717}$, [S II]$_{6731}$
7L	9	[O II]$_{3727}$, H$_\beta$, [O III]$_{4959}$, [O III]$_{5007}$, [N II]$_{6549}$, H$_\alpha$, [N II]$_{6584}$, [S II]$_{6717}$, [S II]$_{6731}$
7S	8	[O II]$_{3727}$, H$_\beta$, [O III]$_{5007}$, [N II]$_{6549}$, H$_\alpha$, [N II]$_{6584}$, [S II]$_{6717}$, [S II]$_{6731}$
8L	5	[O II]$_{3727}$, H$_\beta$, [O III]$_{4959}$, [O III]$_{5007}$, H$_\alpha$
8S	7	[O II]$_{3727}$, H$_\beta$, [N II]$_{6549}$, H$_\alpha$, [N II]$_{6584}$, [S II]$_{6717}$, [S II]$_{6731}$
9L	7	[O II]$_{3727}$, H$_\beta$, [N II]$_{6549}$, H$_\alpha$, [N II]$_{6584}$, [S II]$_{6717}$, [S II]$_{6731}$
9S	6	[O II]$_{3727}$, H$_\beta$, [N II]$_{6549}$, H$_\alpha$, [N II]$_{6584}$, [S II]$_{6717}$
10L	8	[O II]$_{3727}$, H$_\beta$, [O III]$_{5007}$, [N II]$_{6549}$, H$_\alpha$, [N II]$_{6584}$, [S II]$_{6717}$, [S II]$_{6731}$
10S	7	[O II]$_{3727}$, [O III]$_{5007}$, [N II]$_{6549}$, H$_\alpha$, [N II]$_{6584}$, [S II]$_{6717}$, [S II]$_{6731}$
11L	5	[O II]$_{3727}$, H$_\beta$, [O III]$_{4959}$, [O III]$_{5007}$, H$_\alpha$
11S	6	[O II]$_{3727}$, [N II]$_{6549}$, H$_\alpha$, [N II]$_{6584}$, [S II]$_{6717}$, [S II]$_{6731}$
12L	5	[O II]$_{3727}$, H$_\beta$, [N II]$_{6549}$, H$_\alpha$, [N II]$_{6584}$
12S	6	[O II]$_{3727}$, H$_\beta$, H$_\alpha$, [N II]$_{6584}$, [S II]$_{6717}$, [S II]$_{6731}$
13L	9	[O II]$_{3727}$, H$_\beta$, [O III]$_{4959}$, [O III]$_{5007}$, [N II]$_{6549}$, H$_\alpha$, [N II]$_{6584}$, [S II]$_{6717}$, [S II]$_{6731}$
13S	6	[O II]$_{3727}$, H$_\beta$, H$_\alpha$, [N II]$_{6584}$, [S II]$_{6717}$, [S II]$_{6731}$
14L	10	[O II]$_{3727}$, H$_\beta$, [O III]$_{4959}$, [O III]$_{5007}$, [O I]$_{6300}$ [N II]$_{6549}$, H$_\alpha$, [N II]$_{6584}$, [S II]$_{6717}$, [S II]$_{6731}$
14S	7	[O II]$_{3727}$, H$_\beta$, [O III]$_{5007}$, H$_\alpha$, [N II]$_{6584}$, [S II]$_{6717}$, [S II]$_{6731}$
15L	8	[O II]$_{3727}$, H$_\beta$, [O III]$_{5007}$, [N II]$_{6549}$, H$_\alpha$, [N II]$_{6584}$, [S II]$_{6717}$, [S II]$_{6731}$
15S	8	[O II]$_{3727}$, H$_\beta$, [O III]$_{5007}$, [N II]$_{6549}$, H$_\alpha$, [N II]$_{6584}$, [S II]$_{6717}$, [S II]$_{6731}$
16L	5	[O II]$_{3727}$, H$_\beta$, [O III]$_{4959}$, [O III]$_{5007}$, H$_\alpha$,
16S	10	[O II]$_{3727}$, H$_\beta$, [O III]$_{4959}$, [O III]$_{5007}$, [O I]$_{6300}$, [O I]$_{6363}$, [N II]$_{6549}$, H$_\alpha$, [N II]$_{6584}$, [S II]$_{6717}$, [S II]$_{6731}$
17L	7	[O II]$_{3727}$, H$_\beta$, [O III]$_{5007}$, H$_\alpha$, [N II]$_{6584}$, [S II]$_{6717}$, [S II]$_{6731}$
17S	9	[O II]$_{3727}$, H$_\gamma$, H$_\beta$, [O III]$_{4959}$, [O III]$_{5007}$, [O I]$_{6300}$ H$_\alpha$, [N II]$_{6584}$, [S II]$_{6717}$, [S II]$_{6731}$
18L	7	[O II]$_{3727}$, H$_\beta$, [O III]$_{4959}$, [O III]$_{5007}$, H$_\alpha$, [N II]$_{6584}$, [S II]$_{6717}$,
18S	7	[O II]$_{3727}$, H$_\beta$, [N II]$_{6549}$, H$_\alpha$, [N II]$_{6584}$, [S II]$_{6717}$, [S II]$_{6731}$
19L	5	[O II]$_{3727}$, H$_\beta$, H$_\alpha$, [N II]$_{6584}$, [S II]$_{6717}$,
19S	9	[O II]$_{3727}$, H$_\beta$, [O III]$_{5007}$, [O I]$_{6300}$ [N II]$_{6549}$, H$_\alpha$, [N II]$_{6584}$, [S II]$_{6717}$, [S II]$_{6731}$
20L	9	[O II]$_{3727}$, He I$_{4471}$, H$_\beta$, [O III]$_{4959}$, [O III]$_{5007}$, H$_\alpha$, [N II]$_{6584}$, [S II]$_{6717}$, [S II]$_{6731}$
20S	8	[O II]$_{3727}$, H$_\beta$, [O III]$_{5007}$, [N II]$_{6549}$, H$_\alpha$, [N II]$_{6584}$, [S II]$_{6717}$, [S II]$_{6731}$
21L	7	[O II]$_{3727}$, H$_\beta$, [O III]$_{5007}$, H$_\alpha$, [N II]$_{6584}$, [S II]$_{6717}$, [S II]$_{6731}$
21S	7	[O II]$_{3727}$, H$_\beta$, [N II]$_{6549}$, H$_\alpha$, [N II]$_{6584}$, [S II]$_{6717}$, [S II]$_{6731}$
22L	7	[O II]$_{3727}$, H$_\beta$, [O III]$_{4959}$, [O III]$_{5007}$, H$_\alpha$, [S II]$_{6717}$, [S II]$_{6731}$
22S	11	[O II]$_{3727}$, H$_\gamma$, H$_\beta$, [O III]$_{4959}$, [O III]$_{5007}$, He I$_{5875}$ [N II]$_{6549}$, H$_\alpha$, [N II]$_{6584}$, [S II]$_{6717}$, [S II]$_{6731}$
23L	7	[O II]$_{3727}$, H$_\beta$, [O III]$_{5007}$, H$_\alpha$, [N II]$_{6584}$, [S II]$_{6717}$, [S II]$_{6731}$
23S	9	[O II]$_{3727}$, H$_\beta$, [O III]$_{5007}$, O VI$_{5290}$, [N II]$_{6549}$, H$_\alpha$, [N II]$_{6584}$, [S II]$_{6717}$, [S II]$_{6731}$
24L	8	[O II]$_{3727}$, H$_\beta$, [O III]$_{5007}$, [N II]$_{6549}$, H$_\alpha$, [N II]$_{6584}$, [S II]$_{6717}$, [S II]$_{6731}$
24S	8	[O II]$_{3727}$, H$_\gamma$, H$_\beta$, [O III]$_{4959}$, [O III]$_{5007}$, H$_\alpha$, [N II]$_{6584}$, [S II]$_{6717}$
25L	10	[O II]$_{3727}$, H$_\gamma$, H$_\beta$, [O III]$_{4959}$, [O III]$_{5007}$, [N II]$_{6549}$, H$_\alpha$, [N II]$_{6584}$, [S II]$_{6717}$, [S II]$_{6731}$
25S	7	[O II]$_{3727}$, H$_\beta$, [O III]$_{5007}$, H$_\alpha$, [N II]$_{6584}$, [S II]$_{6717}$, [S II]$_{6731}$

other z component present in each spectrum (the discrepant z for GLCS 3, instead is wrong).

All this implies that z duplicity for nine GLCSs (eight with a letter close to z_{NED} and GLCS 7) might have been guessed by means of a careful comparison of discrepant z values reported in different databases. For the remaining 16 GLCSs, however, there is no indication in presently available literature data for the presence of two distinct z components.

Comparison of data in Cols. 3–5 (of Table 2) reveal that the SDSS z measure algorithm has identified the candidate source in 11 cases and the candidate lens in 14 cases. This might sound curious, as one might have expected that the spectral contribution of the lens should have dominated over the one of the sources, the former being both larger and brighter than the latter. We stress, however, that this is not the case as we selected our GLCSs on the basis of a minimum number of emission lines, which we requested to be the same for the candidate lens and source. As a result, both components of our GLCSs are characterized by a conspicuous number of emission lines, as can be seen in Table 3 reporting for each GLC component (Col. 1, where L stands for lens and S stands for source), the number n_{EL} (Col. 2), and type of identified emission lines (Col. 3).

Data in Col. 3 of Table 3 show that in a few cases (1S, 16S, 17S, 20L, 22S, 23S, 24S, and 25L) further identification by RES, which we required for z systems that had reached a score equal to 7, has produced positive results.

Table 4. H_α EW.

GLCS	EW_{SDSS}	EW_{Lens}	EW_{Source}
1	–30	–11	–27*
2	–36	–17	–31*
3	–12	–13*	–12
4	–21	–22*	–17
5	–19	–27	–13*
6	–13	–12*	–13
7	–16	–17*	–18
8	–19	–7	–18*
9	–24	–23*	–8
10	–12	–12*	–18
11	–18	–9	–22*
12	–10	–11*	–12
13	–17	–16*	–10
14	–29	–34*	–21
15	–16	–17*	–11
16	–40	–6	–42*
17	–27	–17	–30*
18	–20	–19	–24*
19	–33	–7	–40*
20	–20	–20*	–16
21	–11	–12*	–14
22	–51	–55*	–12
23	–30	–9	–26*
24	–84	–31	–78*
25	–42	–43*	–21

Detection of the candidate source instead of the candidate lens by the SDSS z measure algorithm may produce failure of the requirement on H_α EW for our candidate lens sample. This actually happens in five cases, listed in Table 4, in which for each GLCS (Col. 1) we reported the value of H_α EW as given by the SDSS (Col. 2) and as we measured for the candidate lens (Col. 3) and source (Col. 4). We rounded values to 1 Å and placed an asterisk close to the value that should be compared to the SDSS value. The agreement between our measures and the SDSS values is quite good ($\langle \Delta EW \rangle = \langle EW_{us} - EW_{SDSS} \rangle = 1.1$ Å, $\sigma_{\langle \Delta EW \rangle} = 5.7$ Å). The five candidate lenses, which have a H_α EW just above our requested value, are 8L, 11L, 16L, 19L, and 23L.

The SDSS images for the 25 GLCSs (listed in Table 1) are shown in Figs. 1 to 3 as a function of their increasing sequential number, which proceeds (through rows) from the upper left corner to the lower right. The cross on each image indicates the position on which the fiber feeding the SDSS spectrograph has been centred. Figures 1 to 3 reveal that in some cases (GLCS 1, 2, 4, 6, 7, 9, 13, 17, 20, 21 and 23) the spectrum has been centred on a bright knot, which is likely to be the background object lensed by the extended galaxy. For most systems, however, the lensed objects are likely to be hidden in the central regions of the lensing galaxies. Figures 1 to 3 reveal also a disky nature, as expected, for the majority of the candidate lensing galaxies (the only exceptions are GLCS 16, 19, 22, and 24 for which the of resolution SDSS images is not enough to establish the presence of the disk).

The last two SDSS images in Fig. 3 show two typical examples of objects that have been discarded, as z duplicity in their spectra could be easily ascribed either to physically related galaxies or to galaxies that are only close in projection. The first object is SDSS J105644.24+321959.9 and the two z components identified by RES in its spectrum ($z_1 = 0.1282$ and $z_2 = 0.1402$) are very likely to be due to the combined contribution of the very close galaxies, which appear to be interacting. A spectrum of the east galaxy is not available in the SDSS, which has identified the low z component of this system, so we cannot attribute the right z to each galaxy. The galaxies appear to be interacting, but might deserve further investigation as their velocity difference ($\Delta cz \simeq 3600$ km s^{-1}) is slightly above the maximum assumed value for close encounters in clusters (Keel et al. 2013). The second object is SDSS J111307.20+050400 ($z_{SDSS} = 0.1150$) and it is easy to interpret z duplicity found by RES ($z_1 = 0.0267$ and $z_2 = 0.1153$) as due to the combined contribution of the background compact object on which SDSS spectrum has been centred, with the outskirts of the foreground large galaxy laying to its north. An SDSS spectrum is available for this latter galaxy (SDSS J111307.90+050422.2) confirming its foreground nature ($z_{SDSS} = 0.0270$)

The SDSS also provides values for the galaxy stellar mass, which are computed following the prescriptions of Maraston et al. (2009), assuming either a star formation model and history or a simple passive evolution, and of Chen et al. (2012), which assume either Bruzual & Charlotte (2003) or Maraston & Stromback (2011) stellar population synthesis models. As galaxy stellar masses are derived on the basis of the spectrum and of its z, we considered reliable only those referring to the 14 objects for which the SDSS detected the candidate lens. We report in Table 5 for each of them: (Col. 1) the stellar mass values (expressed as Log $M/M_\odot$), referring to Maraston et al. (2009) methods (Cols. 2 and 3), and Chen et al. (2012) methods (Cols. 4 and 5). The agreement among the four values for the stellar mass is very good and, as a whole, the candidate lenses demonstrate values for the stellar mass consistent with those shown by spiral galaxies, the only exception is 22L, which shows the lowest stellar mass in the sample.

Finally we computed, for each object in our sample the rest-frame de-reddened $g - r$ colour, finding $\langle g - r \rangle = 0.50$ and $\sigma_{\langle g-r \rangle} = 0.18$. This places our lens candidates well within the blue population of the SDSS galaxies (Strateva et al. 2001; Baldry et al. 2004; Blanton et al. 2003, 2005; Skibba & Sheth 2009), and even somewhat bluer than the AMIGA SDSS sample of Sc isolated galaxies (Fernandez Lorenzo et al. 2012).

4. Activity classification

We set the constraint on H_α EW to ensure a large content of disk galaxies in the GLCS sample, as H_α EW broadly correlates with the galaxy star formation rate (SFR) and, consequently, with the presence and dominance of the disk. A strong H_α emission, however, is not always a signature of an increased star formation, as it might be due to the presence of an active galactic nucleus (AGN), which does not automatically imply the presence of a disk, as morphological studies of AGN host galaxies have so far yielded conflicting results (Kauffmann et al. 2003; Pierce et al. 2007; Choi et al. 2009; Gabor et al. 2009; Povic et al. 2009).

Although SDSS images together with stellar mass estimates and $g - r$ colours confirmed the disky nature of our candidate lenses, we think that activity classification can add a useful piece of information on the whole sample, providing further evidence for the presence of the disk in candidate lensing galaxies and also offering useful information about the nature of the candidate lensed sources.

Classification can be done by means of the standard diagnostic diagrams (Baldwin et al. 1981; Veilleux & Osterbrock 1987; Veilleux 2002), also known as BPT, which have proved to be an extremely efficient method to distinguish the different types of activity encountered in emission line galaxies (Veilleux et al. 1995; Véron et al. 1997; Gonçalves et al. 1999; Juneau et al. 2011). Moreover, since BPT diagrams are based

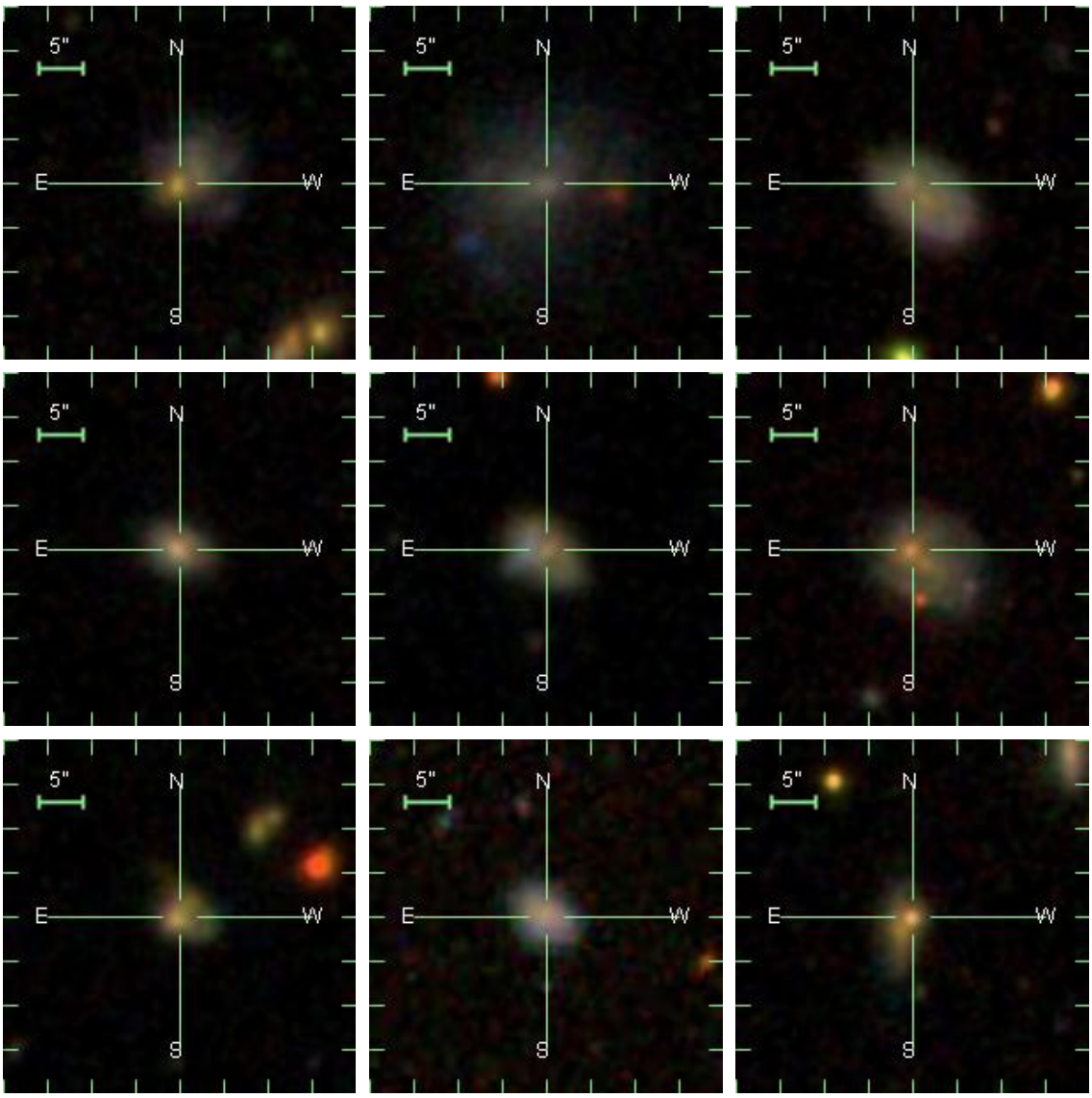

Fig. 1. SDSS images of GLCS 1 (upper left corner) to GLCS 9 (lower right corner).The sequence proceeds through rows (GLCS 3 is in the upper right corner). The cross indicates the position on which the 3″ fiber of the SDSS spectrograph has been centred.

Table 5. Stellar mass estimates for the 14 candidate lens galaxies with $z_{SDSS} = z_L$.

GLC	Log $(M/M_\odot)_1$	Log $(M/M_\odot)_2$	Log $(M/M_\odot)_3$	Log $(M/M_\odot)_4$
3L	10.13	10.32	10.41	10.37
4L	9.64	10.05	10.02	10.06
6L	10.42	10.51	10.91	10.88
7L	10.38	10.72	10.73	10.77
9L	10.12	10.40	10.79	10.84
10L	9.26	9.76	9.87	9.90
12L	10.03	10.24	10.28	10.33
13L	9.47	10.11	10.05	10.09
14L	9.12	9.84	9.53	9.55
15L	9.5	10.06	10.16	10.19
20L	9.01	9.57	9.55	9.56
21L	9.03	9.43	9.50	9.44
22L	7.97	8.45	8.35	8.43
25L	9.12	9.83	9.77	9.69

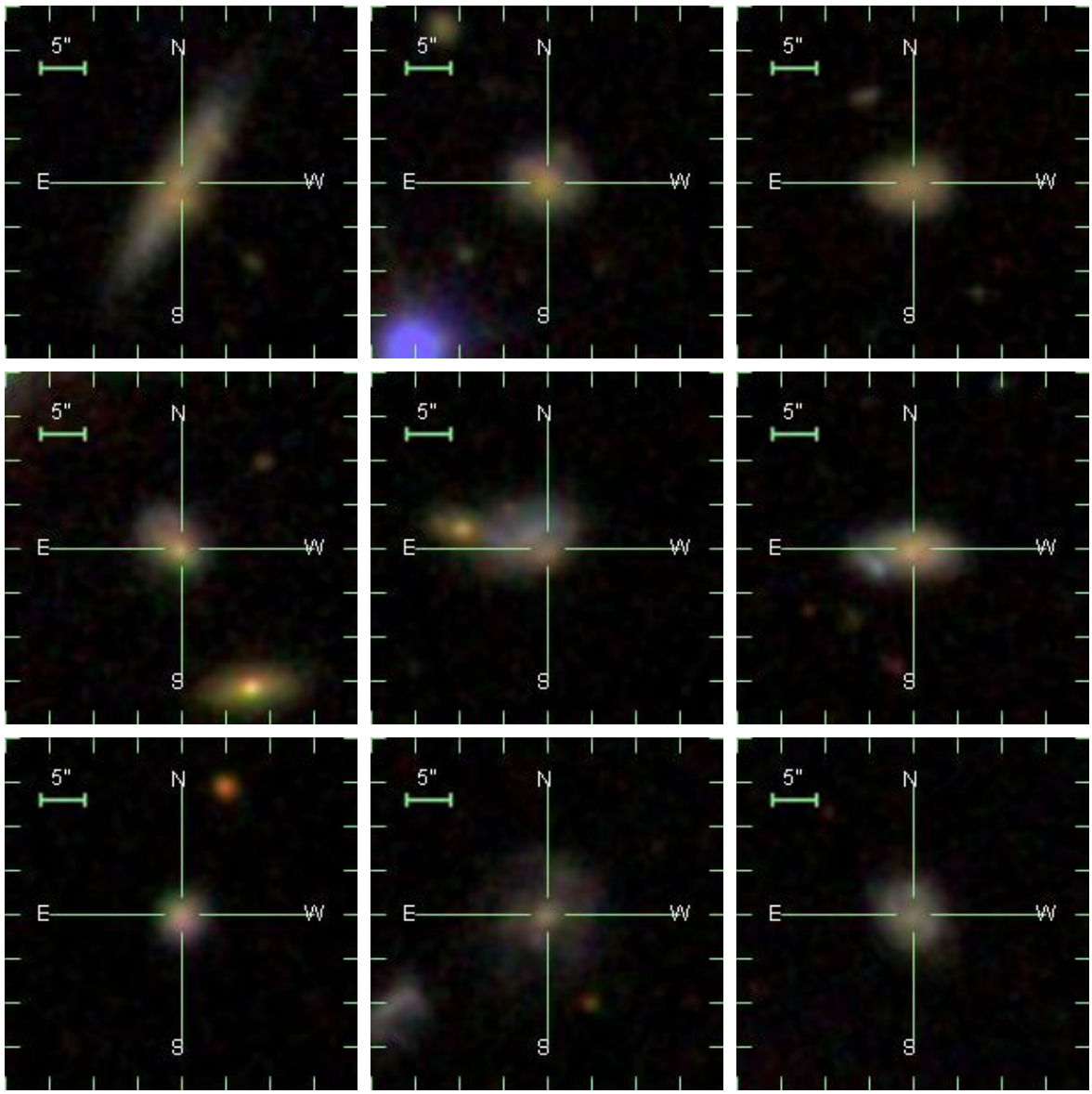

Fig. 2. SDSS images of GLCS 10 to 18. (See Fig. 1 caption for further details.)

on ratios of emission lines that are very close in wavelength, they are almost unaffected by reddening corrections (Veilleux & Osterbrock 1987). According to its position in BPT diagrams, which relate [O III]$_{5007}$/H$_\beta$ to [N II]$_{6583}$/H$_\alpha$, [S II]$_{6717+6731}$/H$_\alpha$ and [O I]$_{6300}$/H$_\alpha$, each galaxy can be classified as AGN (Seyfert or LINER) or Starburst (SB).

Each of us measured the line fluxes needed to produce BPT diagrams independently, making use of IRAF/*splot* task (and taking the average of the two measures). Line flux ratios are reported in Table 3 for those GLC components (of Table 2) that have at least one BPT diagram available. Besides reporting the GLC component identifier (Col. 1), flux ratios, and related uncertainties (Cols. 2 to 5) measured values (and related uncertainties), Table 3 also contains the classification of activity (Col. 6), based on available BPT diagrams. One single classification in Col. 6, when more BPT diagrams are available, indicates that they all agree on it. In case of disagreement, classification is reported accordingly to each available BPT diagram. The upper panels of Fig. 4 show BPT diagnostic diagram 1 (Log [O III]$_{5007}$/H$_\beta$ versus Log [N II]$_{6583}$/H$_\alpha$ hereafter DD1) for lens (left) and lensed candidates (right), the lower panels of Fig. 4 shows the BPT diagnostic diagram 2 (Log [O III]$_{5007}$/H$_\beta$ versus Log [S II]$_{6717+6731}$/H$_\alpha$ hereafter DD2) for lens (left) and lensed candidates (right). The dotted and solid curves in DD1 (upper panels) represent the Kewley et al. (2001, hereafter Kew01) and the Kauffmann et al. (2003, hereafter Kauff03) sequences, which are both supposed to separate SBs (which would lay on their left) from AGNs (which would lay on their right). The difference between the two curves is not surprising since the former curve is theoretical and has been derived using a wide set of models accounting for photo-ionization and stellar population synthesis, while the latter is empirical and was obtained from a large sample (∼22 000) SDSS emission line galaxies. Objects below the Kauff03 sequence are classified as SBs, objects above the Kew01 sequence are classified as AGNs (Seyferts or LINERs), and objects in between the two curves are believed to host a mixture of star formation and AGN and, for this reason, are called composite. The dotted curve and line in DD2 (lower panels of Fig. 4) represents the Kew01 sequence, which separates SB (below) from the AGN (above) region, and the Kewley et al. (2006) sequence (hereafter Kew06), which separates Seyferts (above) from LINERs (below), respectively.

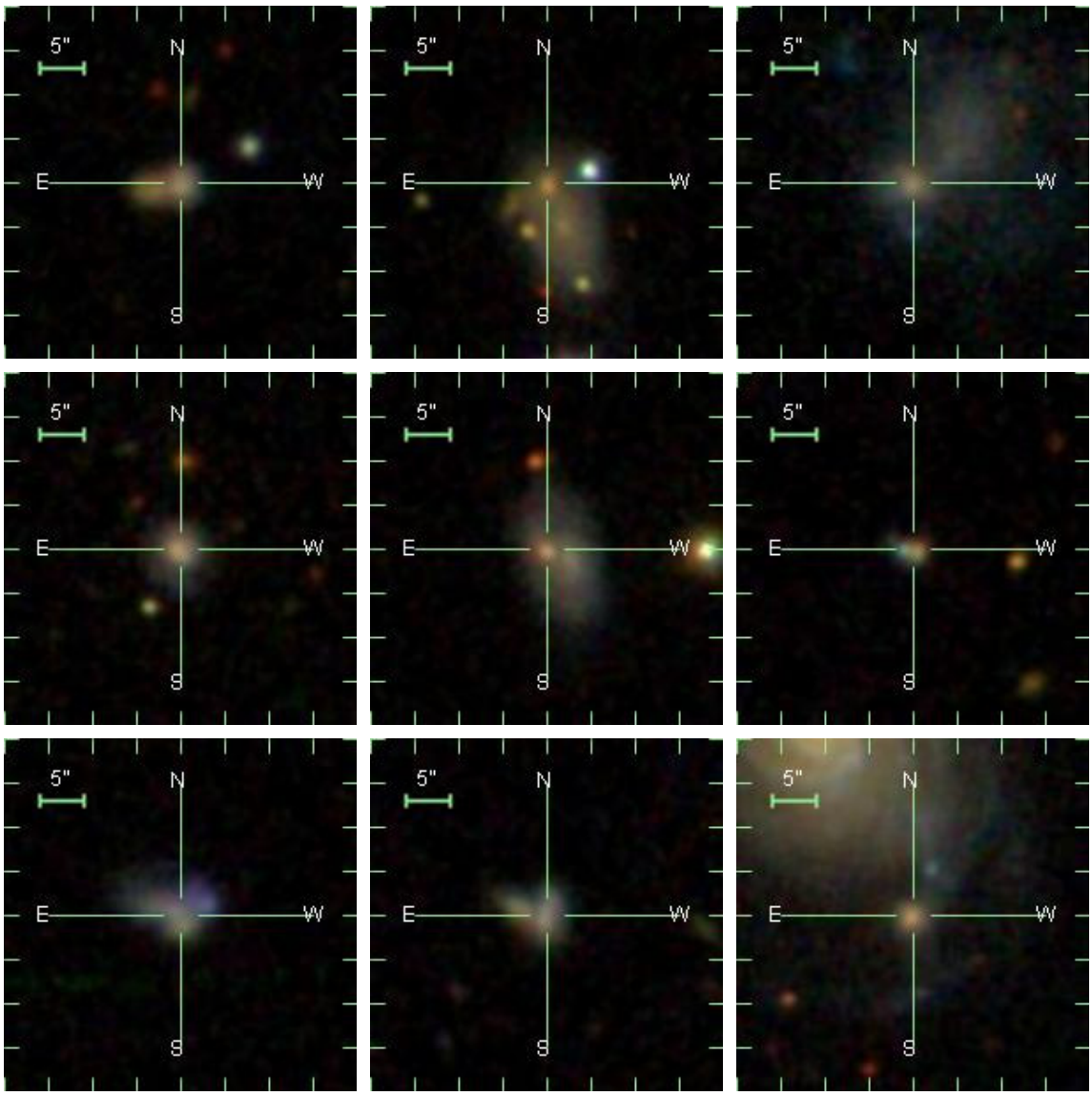

Fig. 3. The first seven images (proceeding through rows as in Figs. 1 and 2) are SDSS images of GLCS 19 to 25. The last two SDSS images show two (of the 29) objects that have been discarded as z duplicity in their spectra cannot be ascribed to gravitational lensing phenomenon.

We do not show the BPT diagnostic diagram 3 (Log $[O\ III]_{5007}/H_\beta$ versus Log $[O\ I]_{6300}/H_\alpha$ hereafter DD3) because too few GLC components have the $[O\ I]_{6300}$ line identified (see Table 3), but we use the data when available (Col. 5 in Table 6) to classify their kind of activity accordingly.

The upper and lower panel at the left of Fig. 4 show that SB is the dominant activity for candidate lensing galaxies. There is only one object (13L) which, according to both diagrams, would be classified as Seyfert, even though it lays close to the border Seyfert SB in DD1 and Seyfert LINER SB in DD2. This object is classified as star forming in the SDSS, which detected the low z component in this spectrum. Two other candidate lenses (20L and 24L) show discordant classifications. Candidate 20L would be classified as SB, according to DD1, and as a Seyfert, according to DD2 (just above the Kew01 curve), and candidate 24L as a SB in DD1 and as a LINER in DD2. The SDSS classification is only available for 20L since SDSS has detected the high z component of GLCS 24), and confirms its star-forming classification. There are another three lens candidates (6L, 10L and 17L), which are classified as composite in DD1 and as SB, LINER, and Seyfert in DD2, respectively (10L and 17L actually lie at the border between Seyfert and LINERS). Following Juneau et al. (2011) they should be classified accordingly to their location in DD2 as it is the nature of a composite object itself which implies classification as AGN (Seyfert or LINER) or as SB in DD2. Unfortunately, the SDSS has detected the high z component in all these three systems so we cannot compare their classification with ours.

As a whole 13/18 candidate lensing galaxies in Table 6 are unambiguously classified as SB corresponding to $\simeq$52% of the total sample. This fraction remarkably agrees with the observed frequency (51%) of SB phenomenon in Sb galaxies (Ho et al. 1997a,b), which the same authors report to be 22% for Sa and 80% for Sc galaxies.

Four (10L, 13L, 17L, and 20L) of the five candidate lensing galaxies missing activity classification show the presence of a disk in the SDSS images (Figs. 2 and 3), while for 24L the classification is uncertain and the SDSS image does not allow us to confirm the presence of a disk.

The right upper and lower panels in Fig. 4 show that two candidate lensed galaxies (1S and 5S) can be unambiguously classified as Seyferts (for 5S the classification holds also

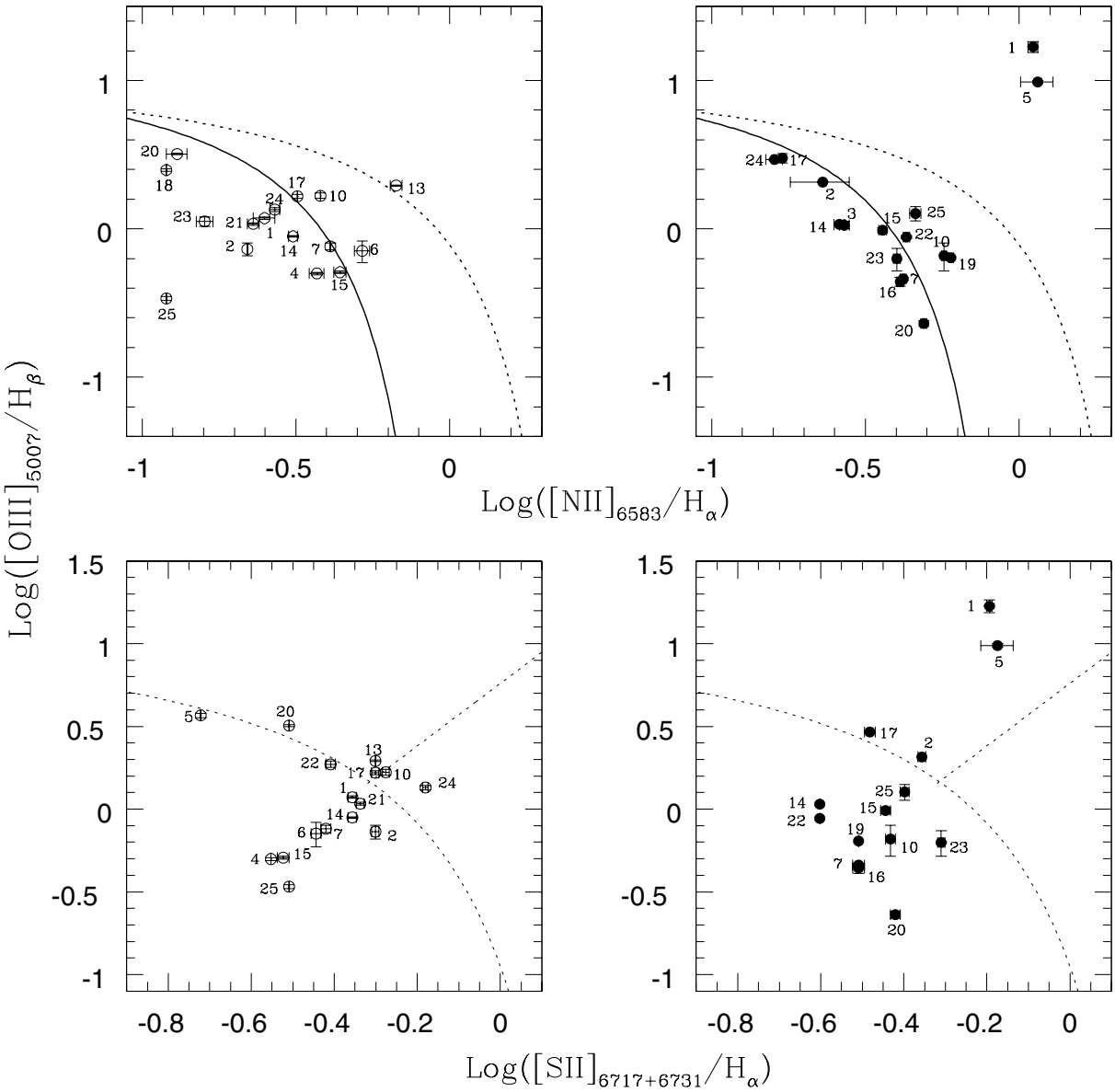

Fig. 4. BPT Diagnostic diagrams DD1 (*upper panels*) and DD2 (*lower panels*) for the lensing (*left*) and lensed (*right*) components in GLCSs.

in DD3). Both objects have been classified as AGN in the SDSS, which detected the high z component in both spectra. Two other objects (2S and 17S) would be classified as SB in DD1 and as Seyfert in DD2 (although they lie rather close to the Kew01 curve). In both cases SDSS detected the high z component and classified them as star forming. There are another four candidate lensed galaxies (10S, 19S, 22S and 25S), which are classified as composite in DD1 and should be classified SB according to DD2. These four objects have been classified either as star forming (10S and 19S) or as SB (22S and 25S) in the SDSS, which has detected the high z component of the spectrum in all four cases.

5. Conclusions

With the aim of increasing the number of disk galaxies acting as gravitational lenses, we have run our original code RES (Redshift for Emission line Spectra) on a large sample of galaxy spectra that we have selected from the SDSS DR 8 requiring an $EW(\mathrm{H}_\alpha) \leq -10$ Å. From the 54 spectra in which RES identified two z systems characterized by a minimum number of four emission lines, we rejected the 29 for which spectral z duplicity could be easily ascribed to combined contribution of two very close galaxies, retaining the 25 that are very likely to be gravitational lens systems. Inspection of available literature revealed that all of them are new (previously unknown), although in 9/25 cases one might have guessed z duplicity through a careful check of z values reported in NED. Visual inspection of SDSS images allowed us to verify that the vast majority (21/25) of candidate lenses is made of disk galaxies, confirming the goodness of our selection criteria. Also stellar mass estimates and $g-r$ rest-frame colour confirm the disky nature of our candidate lenses.

The abundance of emission lines in each lensing and lensed candidates, made it feasible to classify activity type of 18/25 and 16/25, respectively, which resulted to be SB in the majority of cases (12/18 and 11/16). As a whole candidate lenses galaxies show a SB occurrence (13/25), which is typical of Sb galaxies. High-resolution photometry and spectroscopy are needed to confirm the true nature of our GLCSs.

Table 6. Line flux ratios and activity classification for GLC components.

GLC	$[O\ III]_{5007}/H_\beta$	$[N\ II]_{6583}/H_\alpha$	$[S\ II]_{6717+6731}/H_\alpha$	$[O\ I]_{6300}/H_\alpha$	Activity type
1L	1.18 ± 0.10	0.25 ± 0.07	0.44 ± 0.09	–	SB
1S	16.87 ± 1.47	1.11 ± 0.04	0.64 ± 0.01	–	Sy
2L	0.73 ± 0.07	0.22 ± 0.00	0.50 ± 0.01	–	SB
2S	2.07 ± 0.02	0.23 ± 0.05	0.44 ± 0.01	–	SB/Sy
3S	1.06 ± 0.06	0.27 ± 0.01	–	–	SB
4L	0.50 ± 0.01	0.37 ± 0.02	0.28 ± 0.00	–	SB
5L	3.68 ± 0.12	–	0.19 ± 0.00	–	SB
5S	9.76 ± 0.24	1.15 ± 0.14	0.67 ± 0.06	0.07 ± 0.01	Sy
6L	0.71 ± 0.12	0.52 ± 0.03	0.36 ± 0.01	–	composite/SB
7L	0.76 ± 0.04	0.41 ± 0.00	0.38 ± 0.01	–	SB
7S	0.46 ± 0.01	0.42 ± 0.01	0.31 ± 0.01	–	SB
10L	1.67 ± 0.07	0.38 ± 0.00	0.53 ± 0.00	–	composite/LINER
10S	0.66 ± 0.14	0.57 ± 0.01	0.37 ± 0.01	–	composite/SB
13L	1.96 ± 0.02	0.67 ± 0.03	0.50 ± 0.00	–	Sy
14L	0.89 ± 0.01	0.31 ± 0.01	0.44 ± 0.01	0.04 ± 0.0	SB
14S	1.07 ± 0.02	0.26 ± 0.01	0.25 ± 0.00	–	SB
15L	0.51 ± 0.01	0.44 ± 0.02	0.30 ± 0.01	–	SB
15S	0.98 ± 0.04	0.36 ± 0.01	0.36 ± 0.01	–	SB
16S	0.44 ± 0.03	0.41 ± 0.01	0.31 ± 0.01	0.05 ± 0.00	SB
17L	1.66 ± 0.05	0.32 ± 0.00	0.50 ± 0.01	–	composite/Sy
17S	2.93 ± 0.03	0.16 ± 0.01	0.33 ± 0.01	–	SB/Sy
18L	2.49 ± 0.04	0.12 ± 0.00	–	–	SB
19S	0.64 ± 0.01	0.60 ± 0.01	0.31 ± 0.00	0.05 ± 0.00	composite/SB/SB
20L	3.20 ± 0.04	0.13 ± 0.01	0.31 ± 0.00	–	SB/Sy
20S	0.23 ± 0.01	0.49 ± 0.01	0.38 ± 0.01	–	SB
21L	1.08 ± 0.02	0.23 ± 0.01	0.46 ± 0.01	–	SB
22L	1.87± 0.08	–	0.39 ± 0.01	–	SB
22S	0.88 ± 0.02	0.43 ± 0.01	0.25 ± 0.00	–	composite/SB
23L	1.12 ± 0.33	0.16 ± 0.08	–	–	SB
23S	0.63 ± 0.11	0.40 ± 0.01	0.49 ± 0.01	–	SB
24L	1.35 ± 0.04	0.27 ± 0.01	0.66 ± 0.01	–	SB/LINER
24S	3.0 ± 0.21	0.17 ± 0.00	–	–	SB
25L	0.34 ± 0.01	0.12 ± 0.00	0.31 ± 0.00	–	SB
25S	1.27 ± 0.14	0.46 ± 0.02	0.40 ± 0.01	–	composite/SB

Acknowledgements. We would like to thank the anonymous referee for his/her constructive comments and suggestions, which helped us to greatly improve the scientific content of this paper. We acknowledge the usage of SDSS-III. Funding for SDSS-III has been provided by the Alfred P. Sloan Foundation, the Participating Institutions, the National Science Foundation, and the US Department of Energy Office of Science. The SDSS-III web site is http://www.sdss3.org/. SDSS-III is managed by the Astrophysical Research Consortium for the Participating Institutions of the SDSS-III Collaboration including the University of Arizona, the Brazilian Participation Group, Brookhaven National Laboratory, University of Cambridge, Carnegie Mellon University, University of Florida, the French Participation Group, the German Participation Group, Harvard University, the Instituto de Astrofisica de Canarias, the Michigan State/Notre Dame/JINA Participation Group, Johns Hopkins University, Lawrence Berkeley National Laboratory, Max Planck Institute for Astrophysics, Max Planck Institute for Extraterrestrial Physics, New Mexico State University, New York University, Ohio State University, Pennsylvania State University, University of Portsmouth, Princeton University, the Spanish Participation Group, University of Tokyo, University of Utah, Vanderbilt University, University of Virginia, University of Washington, and Yale University. This research has made use of the NASA/IPAC Extragalactic Database (NED) which is operated by the Jet Propulsion Laboratory, California Institute of Technology, under contract with the National Aeronautics and Space Administration. This work has been supported by MIUR.

References

Aihara, H., Allende, P. C., An, D., et al. 2011, ApJS, 193, 29
Allam, S. S., Tucker, D. L., Lin, M. W., et al. 2007, ApJ, 662, 51
Baldwin, J. A., Phillips, M. M., & Terlevich, R. 1981, PASP, 93, 5
Baldry, I. K., Glazebrok, L., Brinkmann, J., et al. 2004, ApJ, 600, 681
Blanton, M. R., Hogg, D. W., Bahcall, N. A., et al. 2003, ApJ, 594, 186
Blanton, M. R., Eisenstein, D., Hogg, D. W., Schlegel, D. W., & Brinkmann, J. 2005, ApJ, 629, 143
Bolton, A. S., Burles, S., Schlegel, D. J., Eisenstein, D. J., & Brinkmann, J. 2004, AJ, 127, 1860
Bolton, A. S., Burles, S., Koopmans, L. V. E., Treu, T., & Moustaras, L. A. 2006, ApJ, 638, 703
Bolton, A. S., Burles, S., Koopmans, L. V. E., et al. 2008, ApJ, 682, 964
Brownstein, J. R., Bolton, A. S., Schlegel, D. J., et al. 2012, ApJ, 744, 41
Bunker, A. J., Moustakas, L. A., & Davis, M. 2000, ApJ, 531, 95
Bruzual, G., & Charlot, S. 2003, MNRAS, 344, 1000
Chen, Y. M., Kauffmann, G., Tremonti, C. A., et al. 2012, MNRAS, 421, 314
Choi, Y. Y., Woo, J. H., & Park, C. 2009, ApJ, 699, 1679
Colless, M., Dalton, G., Maddox, S., et al. 2001, MNRAS, 328, 1039
Dutton, A. A., Brewer, J. B., Marshall, P. L., et al. 2011, MNRAS, 417, 1621
Fernandez Lorenzo, M., Sulentic, J., Verdes-Montenegro, L., et al. 2012, A&A, 540, A47
Feron, C., Hjorth, J., McKean, J., & Samsing, J. 2009, ApJ, 696, 1319
Fukugita, M., & Turner, E. L. 1991, MNRAS, 253, 99
Gabor, J. M., Impey, C. D., Jahnke, K., et al. 2009, ApJ, 691, 705
Gavazzi, R., Treu, T, Koopmans, L. V. E., et al. 2008, ApJ, 677, 1046
Gonçalves, A. C., Véron-Cetty, M.-P., & Véron, P. 1999, A&AS, 135, 437
Hewett, P. C., Warren, S. J., Willis, J. P., et al. 2000, ASP Conf. Ser., 195, 94
Ho, L. C., Filippenko, A. V., & Sargent, W. L. W. 1997a, ApJ, 487, 579
Ho, L. C., Filippenko, A. V., & Sargent, W L W. 1997b, ApJ, 487, 591
Jiang, G., & Kochanek, C. S. 2007, ApJ, 671, 1568
Juneau, S., Dickinson M., Alexander D. M., & Salim, S. 2011, ApJ, 736, 104
Kauffmann, G., Heckman, T. M., Tremonti, C., et al. 2003, MNRAS, 346, 1055
Kassiola, A., & Kovner, I. 1993, ApJ, 417, 450
Keel, W. C., Manning, A. M., Holwerda, B. W., et al. 2013, PASP, 125, 2
Keeton, C. R., & Kochanek, C. S. 1998, ApJ, 495, 157
Kennicutt, R. C. Jr. 1998, ARA&A, 36, 189
Kewley, L., Dopita, M., Sutherland, R., Heisler, C., & Trevena, J. 2001, ApJ, 556, 121

Kewley, L., Groves, B., Kauffmann, G., & Heckman, T. 2006, MNRAS, 372, 961
Kochanek, C. S. 1991, ApJ, 373, 354
Kochanek, C. S. 1993, ApJ, 417, 438
Kochanek, C. S. 1996, ApJ, 466, 638
Kochanek, C. S., Keeton, C. R., & McLeod, B. A. 2001, ApJ, 547, 50
Koopmans, L. V. E. 2005, MNRAS, 363, 1136
Koopmans, L. V. E., Treu, T., Bolton, A. S., Burles, S., & Moustakas, L. A. 2006, ApJ, 649, 599
Kormann, R., Schneider, P., & Bartelmann, M. 1994, A&A, 284, 285
Majerotto E., Guzzo, L., Samushia, W. J., et al. 2012, MNRAS, 424, 1392
Maller, A. H., Simard, L., Guhathakurta, P., et al. 2000, ApJ, 533, 194
Maoz, D., & Rix, H. W. 1993, ApJ, 416, 425
Maraston, C., & Stromback, G. 2011, MNRAS, 418, 2785
Maraston, C., Stromback, G., Thomas, D., Wake, D. A., & Nichol, R. C. 2009, MNRAS, 394, L107
Marshall, P. J., Treu, T., Melbourne, J., et al. 2007, ApJ, 671, 1196
Oguri, M. 2007, ApJ, 660, 1
Pierce, C. M., Lotz, J. M., Laird, E. S., et al. 2007, ApJ, 660, L19
Poindexter, S., Morgan, N., & Kochanek, C. S. 2008, ApJ, 673, 34
Povic, M., Sanchez-Portal, M., Perez Garcia, A. M., et al. 2009, ApJ, 706, 810
Refsdal, S. 1964, MNRAS, 128, 307
Roche, N., Franzetti, P., Garilli, B., et al. 2012, MNRAS, 420, 1764
Rusin, D., & Kochanek, C. S. 2005, ApJ, 623, 666
Skibba, R. A., & Sheth, R. K. 2009, MNRAS, 392, 1080
Smail, I., Swinbank, A. M., Richard, J., et al. 2007, ApJ, 654, 33
Strateva, I., Zeliko, I., Knapp, G. R., et al. 2001, ApJ, 122, 1861
Turner, E. L., Ostriker, J. P., & Gott, J. R. III 1984, ApJ, 284, 1
Treu, T., Koopmans, L. V. E., Bolton, A. S., Burles, S., & Moustakas, L. A. 2006, ApJ, 640, 662
Veilleux, S. 2002, in AGN Surveys, eds. R. F. Green, E. Ye. Khachikian, & D. B.Sanders, IAU Coll. 184, ASP Conf. Proc., 284, 111
Veilleux, S., & Osterbrock, D. E. 1987, ApJS, 63, 295
Veilleux, S., Kim, D. C., Sanders, D. B., Mazzarella, J. M., & Soifer, B. T. 1995, ApJS, 98, 171
Véron, P., Gonçalves, A. C., & Véron-Cetty, M.-P. 1997, A&A, 319, 52
Willis, J. P., Hewett, P. C., & Warren, S. J. 2005, MNRAS, 363, 1369
Willis, J. P., Hewett, P. C., Warren, S. J., Dye, S., & Maddox, N. 2006, MNRAS, 369, 1521
York, D. G., Adelman, J., Anderson, J. E. Jr., et al. 2000, AJ, 120, 1579